*Nucleic Acids Research*, 2024, **52**, e41
https://doi.org/10.1093/nar/gkae202
Advance access publication date: 30 March 2024
**Methods**

# Live-cell imaging of human apurinic/apyrimidinic endonuclease 1 in the nucleus and nucleolus using a chaperone@DNA probe

**Xiangjian Cao†, Jinghui Zheng†, Ruilan Zhang†, Ying Sun and Meiping Zhao ***

Beijing National Laboratory for Molecular Sciences and MOE Key Laboratory of Bioorganic Chemistry and Molecular Engineering, College of Chemistry and Molecular Engineering, Peking University, Beijing 100871, China

*To whom correspondence should be addressed. Tel: +86 10 62758153; Fax: +86 10 62751708; Email: mpzhao@pku.edu.cn
†The first three authors should be regarded as Joint First Authors.

## Abstract

Human apurinic/apyrimidinic endonuclease 1 (APE1) plays crucial roles in repairing DNA damage and regulating RNA in the nucleus. However, direct visualization of nuclear APE1 in live cells remains challenging. Here, we report a chaperone@DNA probe for live-cell imaging of APE1 in the nucleus and nucleolus in real time. The probe is based on an assembly of phenylboronic acid modified avidin and biotin-labeled DNA containing an abasic site (named PB-ACP), which cleverly protects DNA from being nonspecifically destroyed while enabling targeted delivery of the probe to the nucleus. The PB-ACP construct specifically detects APE1 due to the high binding affinity of APE1 for both avidin and the abasic site in DNA. It is easy to prepare, biocompatible and allowing for long-term observation of APE1 activity. This molecular tool offers a powerful means to investigate the behavior of APE1 in the nuclei of various types of live cells, particularly for the development of improved cancer therapies targeting this protein.

## Graphical abstract

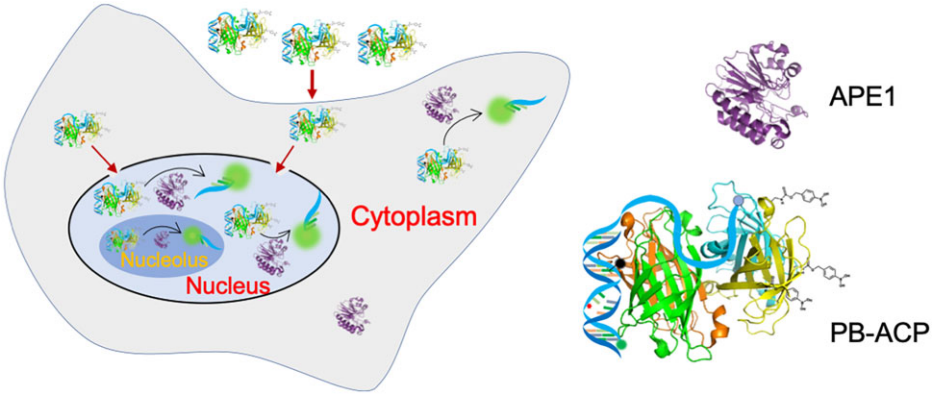


## Introduction

Human apurinic/apyrimidinic endonuclease 1 (APE1) is a multifunctional protein which plays critical roles in repairing DNA damage and controlling other important intracellular processes (1,2). Its subcellular localization and diverse functions, including regulating apoptosis, proliferation, and differentiation, make it a target of intense research (3). In the nucleus, APE1 acts as the major AP endonuclease, essential for maintaining genome stability (4). As a redox signaling protein, APE1 regulates the transcriptional activity of a number of transcription factors which are key contributors to many diseases (5). Its role in RNA metabolism has also been identified (6). Alterations in the expression, subcellular localization, and activities of APE1 have been reported to be associated with neurodegeneration, cardiovascular disease and the ability of tumor cells to grow and metastasize (7,8). In addition to being used as a predictive and prognostic biomarker for various cancers, APE1 also has been utilized as a therapeutic target due to its critical role as a cellular signaling node in tumor cells (3). Although methods for visualizing APE1 in the cytoplasm of living cells have been well-established (9–11), direct observation of APE1 in the nucleus remains a significant challenge due to limited available molecular tools. Traditional methods like immunofluorescence can only visualize fixed cells (12). Genetically encoded fluorescent probes, such as GFP-tagged proteins, are valuable tools for real-time monitoring of

**Received:** June 17, 2023. **Editorial Decision:** February 27, 2024. **Accepted:** March 7, 2024
© The Author(s) 2024. Published by Oxford University Press on behalf of Nucleic Acids Research.
This is an Open Access article distributed under the terms of the Creative Commons Attribution-NonCommercial License (http://creativecommons.org/licenses/by-nc/4.0/), which permits non-commercial re-use, distribution, and reproduction in any medium, provided the original work is properly cited. For commercial re-use, please contact journals.permissions@oup.com

protein dynamics in living cells over longer time scales (13–15). However, tagging the protein may alter its spatial localization from the native distribution of the untagged protein within the cell. Additionally, the introduction of GFP-tagged APE1 represents an overexpression in cells, which may result in a distribution distinct from the endogenous APE1 alone.

Histones and protamines are nuclear basic proteins that tend to bind to the phosphate backbone of DNA and fold it into a toroid-shaped structure (16). Similar condensation effect of DNA has also been observed for avidin (AVD) with a binding length of 18±4 bp DNA per AVD (17). Interestingly, our previous work disclosed that AVD-assembled biotin-labeled AP site-containing DNA (AP-DNA) on the surface of silica coated magnetic nanoparticles was resistant to many nucleases, whereas can be efficiently cleaved by APE1 (9). These results implied special interactions between AVD and APE1. Our further study revealed that the biotin label not only anchored the AP-DNA probe on avidin, but also substantially increased the binding affinity of AVD for APE1. Based on these inherent molecular properties, we envision that chemically modified AVD may serve as a chaperone of DNA for regulation the reactions between DNA and other molecules.

In this work, we demonstrate a novel type of chaperone@DNA probe which enabled visualization of APE1 in the nucleus of living cells. As illustrated in Scheme 1A, the basic structure of AVD/AP-DNA complex probe (ACP) consists of a biotin-labeled DNA duplex (37 nt/21nt) probe containing an abasic site that is conjugated to avidin at a 1:1 ratio. This probe showed very high sensitivity and specificity to APE1 and allowed quantification of APE1 activity in subcellular compartments and exosomes of different cell types without the need of additional purification steps. By pre-modification of AVD with phenylboronic acid (PB-AVD), the resultant probe is named PB-ACP (Scheme 1B), in which the PB-AVD functions as a chaperone, protecting the DNA strand from nonspecific degradation while enabling effective nuclear targeting delivery of the probe via the importin α/β pathway (Scheme 1C). PB-ACP specifically detects APE1 due to the high binding affinity between avidin and APE1 and the high binding affinity of APE1 for the abasic site in DNA. Using PB-ACP, we visualized APE1 in the nucleus of live cells, including its distribution within the nucleolus, and observed variations in its activity under different conditions. This innovative approach provides a valuable tool for studying the role of APE1 in maintaining genome stability and other cellular processes, as well as for improving cancer treatments.

## Materials and methods

### Materials

The DNA oligonucleotides were synthesized and purified by HPLC (Sangon Biotech Co., China). The sequences of all the DNA strands that have been studied in this work are summarized in Supplementary Table S1. Apurinic/apyrimidinic endonuclease 1 (APE1), Deoxyribonuclease I (DNase I), Exonuclease III (Exo III), Exonuclease I (Exo I), T5 Exonuclease (T5 Exo), Endonuclease IV (Endo IV)and their reaction buffers (Supplementary Table S2) were all purchased from New England Biolabs (NEB, USA). Recombinant Three Prime Repair Exonuclease 1 (TREX1) and its reaction buffer were produced as described by Silva et al. (18). Avidin (AVD) was purchased from Sigma chemical Co. (St. Louis. MO). 4-nitrophenyl chloroform and (hydroxymethyl) phenylboronic acid pinacol ester ((4-(4,4,5,5-tetramethyl-1,3,2-dioxaborolan-2-yl) phenyl) methanol) (PBN) were purchased from Konoscience (Beijing, China).

Mammary gland epithelial adenocarcinoma cells (MCF-7) cell line, Rat adrenal pheochromocytoma cells (PC-12) cell line and PC-12 (highly differentiated) cell special medium (CM-0481) were purchased from Procell Life Science&Technology Co. Ltd (Wuhan, China). Mammary gland epithelial cells (MCF 10A) cell line was purchased from iCell Bioscience Inc (Shanghai, China). Human cervical carcinoma cell line (HeLa), Human Embryonic Kidney 293 cell (HEK-293T) and Adenocarcinomic human alveolar basal epithelial cell line (A549) were purchased from ATCC (Manassas, VA, USA). The human esophageal squamous cell carcinoma cell lines TE-1 wild-type (TE-1 WT) and TE-1 APE1-knockout (TE-1 APE1-KO), along with the TE-1-specific medium, were acquired from Hycyte, Suzhou Haixing Bioscience Co. (Suzhou, China). Mammary Epithelial Cell Growth Medium (MEGM, CC-3150) was purchased from Lonza Bioscience (Basel, Switzerland). Dulbecco's modified Eagle's medium (DMEM), Dulbecco's phosphate buffer solution without calcium & magnesium (DPBS), and F-12 Nutrient Mix were purchased from Corning (Manassas, VA, USA). Human recombinant insulin was purchased from Coolaber (Beijing, China).

### Construction of the AVD/AP-DNA complex (ACP) and measurement of APE1 in protein extracts from different cell types using ACP

The fluorescently labeled AP site-containing dsDNA probe (P1) was designed based on our previous work with some modifications (Supplementary Table S1) (9,18,19). P2-biotin has the same sequence as P1, but with a 3′-biotin tag. To generate the corresponding AVD/AP-DNA complex P1 or P2-biotin were mixed with AVD at a molar ratio of 1:1 and incubated at 37°C for 30 min.

The response of the resultant AVD/AP-DNA complex to APE1 was measured in NEB Buffer 4 with a total volume fixed at 50 μl. APE1 standard solutions or cellular extracts were first diluted to the proper concentrations using NEB Buffer 4 containing 0.04% Triton X-100. In a 200 μl PCR tube, 10 μl of 1 μM ACP and 5 μl of 10× NEB Buffer 4 were added and brought up to a volume of 48 μl with deionized water. Then 2 μl of APE1 standard or cellular extract solution was added to the mixture solution, and immediately measured on a Rotor-Gene Q 5plex HRM Instrument (QIAGEN, Germany). Fluorescence intensity was measured once a cycle (5 s per cycle) with a gain level of 8. The excitation/emission wavelengths were 470 nm/510 nm for FAM, and 585 nm/610 nm for ROX, respectively.

To measure the response of the obtained ACP to other enzymes, the optimal buffer for the tested enzyme shown in Supplementary Table S2 was used instead of Buffer 4. The final concentration of ACP was fixed at 200 nM, and 2 μl of the enzyme solution to be tested was added for the detection.

### Synthesis of PBN and modification of AVD with PBN

The (Hydroxymethyl) phenylboronic acid pinacol ester (0.50 g, 2.1 mmol) was dissolved in 20 ml anhydrous tetrahydrofuran (THF). Next, 0.6 ml (4.3 mmol) of triethylamine was added, followed by 4-nitrophenyl chloroformate (0.47 g,

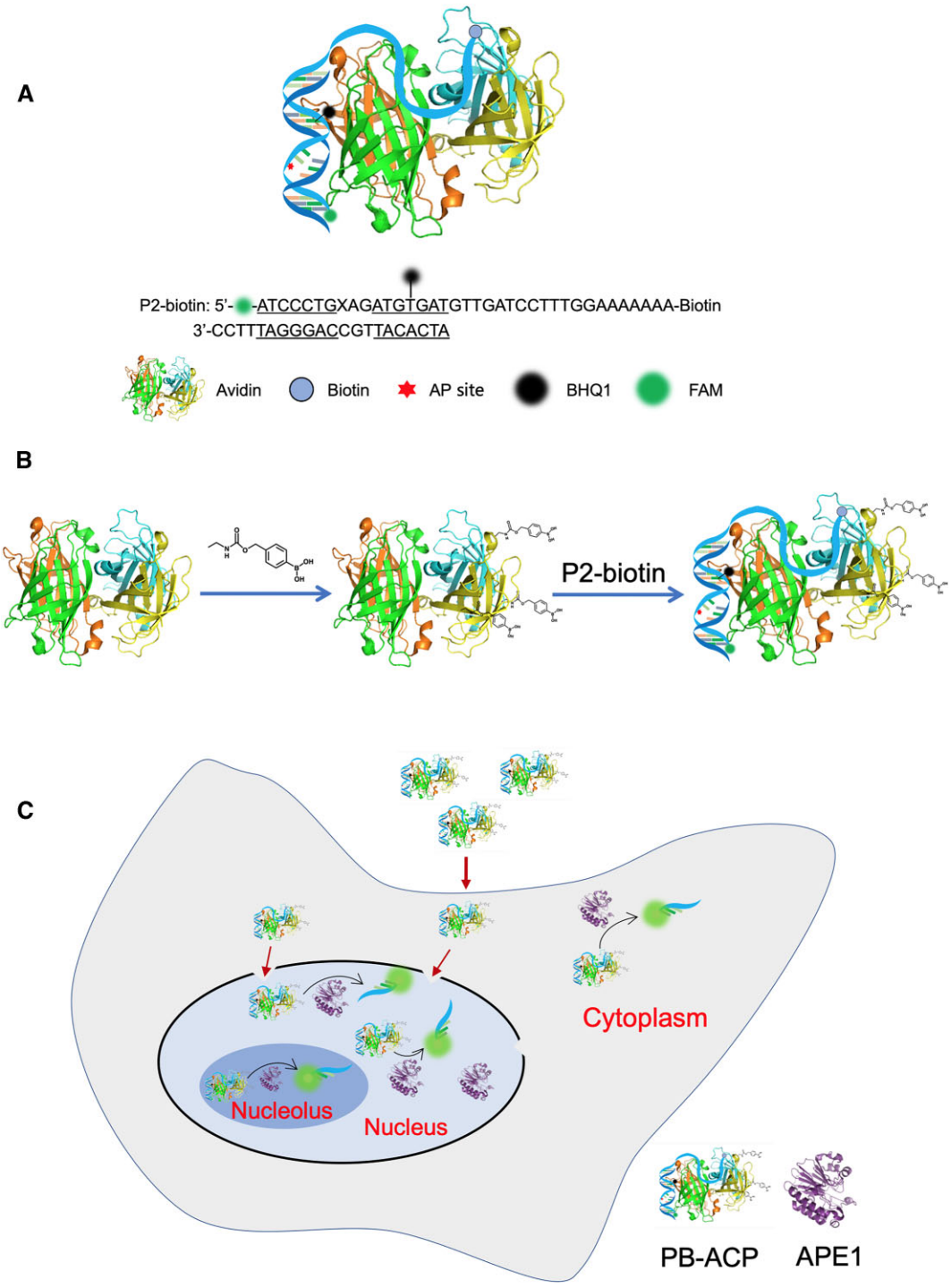


**Scheme 1.** (**A**) Schematic illustration of the AVD/AP-DNA complex probe (ACP) at a conjugation ratio of 1:1. (**B**) Construction of PB-ACP by modification of AVD with phenylboronic acid. (**C**) Visualization APE1 in the nucleus and nucleolus using the PB-ACP-based chaperone@DNA probe.

2.3 mmol), and stirred for 1 h at room temperature. The THF was removed by rotary evaporation, and the dispersion was redissolved in ethyl acetate (EA). After being washed with 1.0 M HCl (50 ml × 3 times) and subsequently with saturated $NaHCO_3$ (50 ml × 3 times), the organic layer was separated by extraction, dried over $MgSO_4$, filtered, and concentrated. The column was eluted with a developing reagent ratio of petroleum ether (PE):EA = 4:1. The obtained product was a white solid, named 4-nitrophenyl 4-(4,4,5,5-tetramethyl-1,3,2-dioxaborolan-2-yl)benzyl carbonate (PBN), with a yield of 0.214 g (25.5%). $^1$H NMR (400 MHz, $CDCl_3$) δ 8.27 (d, $J$ = 9.2 Hz, 2H), 7.85 (d, J = 8.0 Hz, 2H), 7.44 (d, $J$ = 8.1 Hz, 2H), 7.38 (d, $J$ = 9.2 Hz, 2H), 1.35 (s, 12H).

To prepare PB modified ACP (PB-ACP), 50 μl $NaHCO_3$ solution (0.5 M, pH 8.5) was added to 200 μl of AVD solution (2.5 mg/ml) as the buffer, followed by addition of 0.4 mg PBN in DMSO. The reaction proceeded for 2 h at room temperature. The resulting solution containing PB-ACP products was ultra-filtrated using a 10 K filter and washed more than three times with DNase/RNase-free deionized water.

### MALDI-TOF mass spectrometric characterization

Matrix-assisted laser desorption/ionization with time-of-flight mass spectrometry (MALDI-TOF MS) analysis was conducted using an ABI SCIEX 5800 MALDI-TOF/TOF (AB SCIEX, USA) equipped with a 349-nm solid-state laser. Sinapic acid in a 60% acetonitrile/40% $H_2O$ (v/v) matrix was used for sample preparation. Samples were dissolved in an equal volume of matrix solution and spotted on a MALDI plate, then air-dried as per the manufacturer's instructions. Protonation dissociation of the samples was induced using a 349 nm laser. All mass spectra were acquired in linear positive-ion mode with a delay time of 2500 ns.

### Cell transfection of PB-ACP for fluorescence imaging

The cells in a 24-well plate were washed with PBS buffer, followed by addition of 400 μl of Opti-MEM™ medium to each well. To 25 μl of Opti-MEM™ medium, 1.5 μl of Lipofectamine™ 3000 reagent (or 1 μl RNATransMate (Sangon, Shanghai, China) for TE-1 WT and TE-1 APE1-KO cells) was added and mixed well by pipetting. To 25 μl of Opti-MEM™ medium containing 500 ng of DNA in PB-ACP, 1 μl of P3000™ reagent was added and mixed well by pipetting (Note: For TE-1 WT and TE-1 APE1-KO cells transfected with RNATransMate, the addition of P3000™ reagent is not required). The above two solutions were mixed well and allowed to stand at room temperature for 15 min. Then the obtained mixture was added to the cells in the 24-well plate and incubated in a 37°C, 5% $CO_2$/95% air incubator for transfection. After 4 h, the cells were washed with PBS for three times. The nuclei were stained by incubating the cells with Hoechst 33342 Staining Solution for Live Cells (Beyotime, Shanghai, China) for 10 min. Finally, 400 μl of FluoroBrite™ DMEM imaging medium with low fluorescence background was added for imaging.

The A1R Si laser scanning confocal microscope (CLSM), equipped with a 60× oil objective lens, was used to capture the images of the cells using multiple laser channels in synchronized fashion (using open anti-string color mode). When conducting time-lapse fluorescence imaging, the cells to be imaged were transferred to an in-line live cell culture device (37°C, 5% CO2/95% air).

To investigate the alterations of APE1 within the nuclei of living cells under various treatments, stimulation reagents were added to the normal medium at final concentrations of 200 μM for *tert*-butyl-hydroperoxide (tBHP), 100 μM for *cis*-diamminedichloroplatinum (CDDP), 5 mM for *S*-nitrosoglutathion (GSNO), 75 ng/ml for lipopolysaccharide (LPS) and 100 μM for methyl methanesulfonate (MMS), respectively. The treatment duration was 1 h for tBHP and 2 h for the other reagents. Following treatment, the medium was replaced with Opti-MEM™ for subsequent imaging experiments. The concentration of PB-ACP used in the fluorescence imaging experiments was 66 nM.

## Results and discussion

### Specific interactions between AVD/AP-DNA complex probe (ACP) and APE1

Avidin (AVD) is a positively charged homotetrameric biotin-binding glycoprotein (68 kDa, p*I* 10.5). In contrast to its structural and functional analogue streptavidin, both AVD and its complex with biotin bind to DNA with high affinity (17). Interestingly, our previous research revealed that biotin-labeled AP-DNA assembled by AVD pre-immobilized on the surface of SiMNPs was well protected from degradation by various nucleases except APE1(9).

To clarify the mechanism of this discrimination effect, we compared the digestion rates of an AP-DNA probe (P1, 37nt/21nt, Supplementary Table S1) by APE1 and DNase I (a nonspecific endonuclease) in the presence of different amounts of AVD. From Figure 1A, it can be observed that the cleavage rate of P1 by APE1 was almost unaffected by the addition of AVD, while the digestion of P1 by DNase I was notably inhibited when AVD/DNA ratio increased to higher than 1.0. As DNase I mainly interacts with DNA via the ionic interactions between the positively charged amino acids and the backbone phosphates of DNA, these results indicated that the access of DNase I to the DNA strand was significantly prohibited by the tight binding of P1 by AVD.

To explain the capability of APE1 in cleavage of AP-DNA bound by avidin, we performed single-molecule fluorescence resonance energy transfer (smFRET) analysis to investigate the effect of APE1 on the binding of AP-DNA by AVD (Figure 1B). Upon the addition of APE1, the dwell time of AP-DNA on immobilized AVD notably decreased from 22 s to 15 s, indicating that APE1 efficiently bound to the AP sites in DNA. These results are consistent with the reported DNA sculpting mechanism used by APE1 in processing the solvent-exposed AP site in nucleosomal DNA (20).

Previous studies have revealed that biotin binding induces conformational changes in the long loop (residues 36-44) of AVD, leading to its ordered structure and locking the biotin-binding pocket of AVD (21). Furthermore, biotin binding has been observed to enhance the affinity of avidin for DNA (17). The AVD-biotin complex also exhibits high resistance to various proteolytic enzymes (22). In this study, we explored the impact of biotin binding on the interactions between avidin and APE1. The results from isothermal titration calorimetry (ITC) analysis, as presented in Figure 1C, indicated that the presence of biotin at a molar ratio of 4:1 significantly enhanced the binding affinity of AVD for APE1 by approximately 6-fold. It is speculated that the specific binding interface between AVD and APE1 is closely associated with the biotin-binding region of AVD. The conformation and surface amino acid distribution of AVD after binding of biotin are more conducive to the interaction between these two proteins. A more comprehensive investigation of the AVD-APE1 interaction based on multi-faceted approaches will be detailed in a separate report.

Based on above results, anchoring the DNA probe on avidin via a biotin label is beneficial for both the formation of stable assembly of AVD/AP-DNA and the recruitment of APE1 by AVD. We prepared P2-biotin by labeling P1 with biotin at the 3′ end. Interestingly, the addition of avidin at a ratio lower than 0.5 (avidin/P2-biotin) slightly accelerated the digestion rate by APE1, while a further increase of the ratio to higher than 1.0 slightly decreased the reaction rate (Figure 1D). By contrast, the digestion of P2-biotin by DNase I was consistently inhibited in the presence of AVD. When the AVD/P2-biotin ratio increased to higher than 1.0, the digestion of P2-biotin by DNase I was almost completely inhibited, and the discrimination factor between APE1 and DNase I reached the maximum.

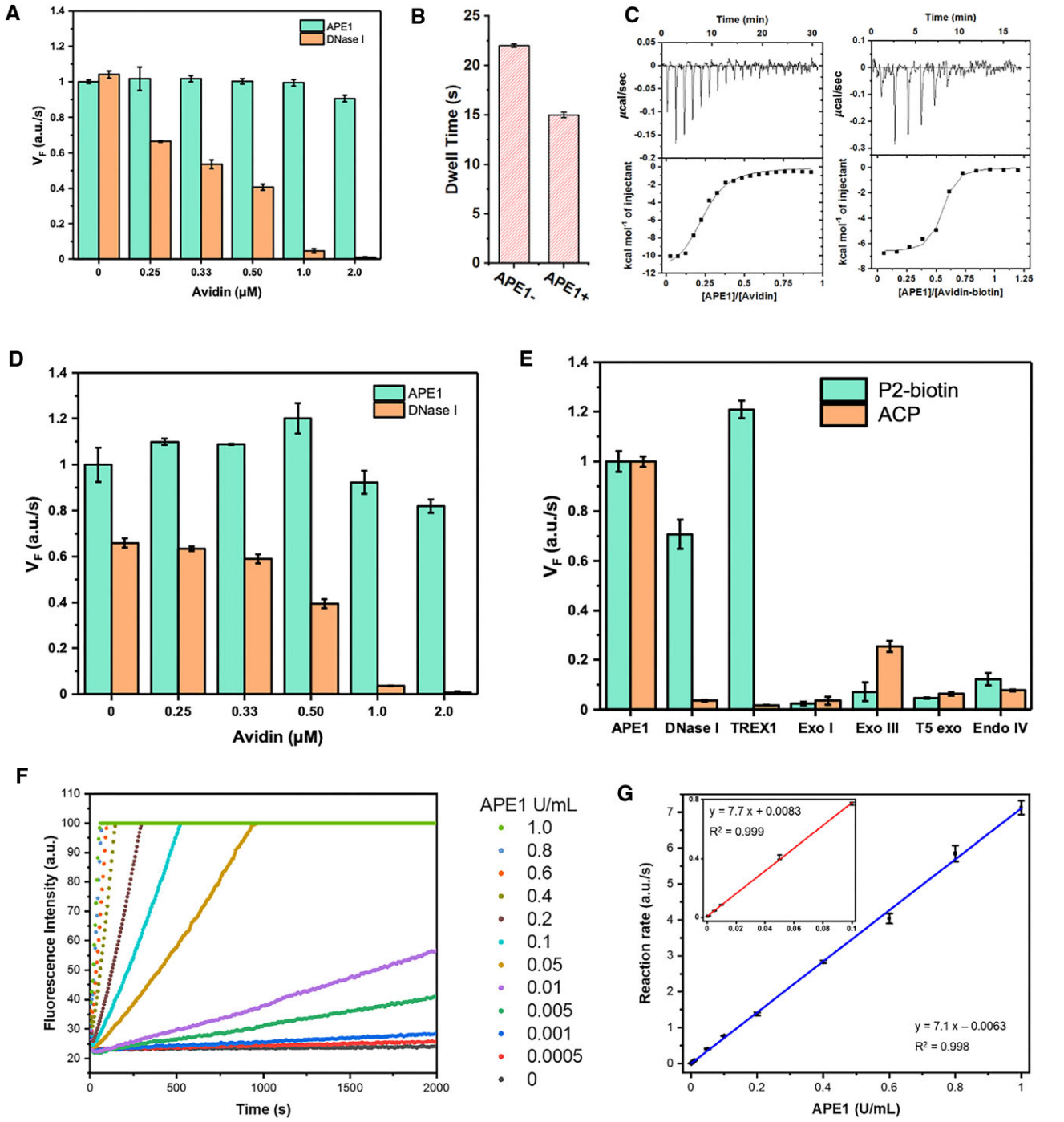


**Figure 1.** (**A**) Comparison of the digestion rates of AP-site containing DNA duplex (P1, Supplementary Table S1) by APE1 (0.5 U/ml) and DNase I (0.5 U/ml) in the presence of different concentrations of AVD. The data were normalized with the digestion rate of the tested probe by APE1 in the absence of AVD set to 1.0. (**B**) Dwell time of AP-DNA on immobilized AVD in the absence and presence of APE1. Data obtained by single-molecule fluorescence resonance energy transfer (smFRET) analysis. (**C**) ITC analysis of the interactions between avidin and APE1 in the absence and presence of biotin. (**D**) Comparison of the digestion rates of P2-biotin (Supplementary Table S1) by APE1 (0.5 U/ml) and DNase I (0.5 U/ml) in the presence of different concentrations of AVD. The data were normalized with the digestion rate of the tested probe by APE1 in the absence of AVD set to 1.0. (**E**) Selectivity of ACP (200 nM) for APE1 over other nucleases tested in their respective optimal buffers. Concentration: APE1 (1.0 U/ml, 33 pM), DNase I (1.0 U/ml, 685 pM), TREX 1 (55 nM), Exo I (2.5 U/ml, 340 pM), Exo III (20 U/ml, 3.96 nM), T5 Exo (1.0 U/ml, 114 pM), Endo IV (1.0 U/ml, 3.23 pM). (**F**) Fluorescence responses of ACP (200 nM) to APE1 at different concentrations in Buffer 4 + 0.002% Triton X-100. (**G**) Linear calibration curve for detection of the activity of APE1. The linear working range is from 0.002 to 1.0 U/ml and the detection limit is 0.0005 U/ml. All experiments were repeated at least three times.

Then we altered the distance between AP site and the biotin labeled 3′ end from 29 nt (P2-biotin) to 22 nt (P3-biotin) and 9 nt (P4-biotin), respectively. As shown in Supplementary Figure S1 and S2, the cleavage rates of P3-biotin and P4-biotin by APE1 both started to decrease at an AVD/AP-DNA ratio larger than 0.5, indicating that the position of AP site from the biotin-binding pocket of avidin was critical for the interactions between APE1 and the AP-DNA. Accordingly, using P2-biotin as the AP-DNA, we prepared AVD/AP-DNA complex probe (denoted as ACP) at a conjugation ratio of 1:1 (Scheme 1A).

We further investigated the discrimination capability of ACP against other typical nucleases with P2-biotin as a control (Figure 1E). Three Prime Repair Exonuclease 1 (TREX1) is the most abundant 3′ exonuclease in mammalian cells, which hydrolyzes both ssDNA and dsDNA (23). Under the tested concentrations, it digested P2-biotin very rapidly, and the signals were even higher than those of APE1. By contrast, ACP showed strong resistance to the degradation by TREX1, indicating excellent protective effect of avidin on the assembled DNA. A similar effect could be seen for DNase I. For other exonucleases such as Exo I and T5 exo, both P2-biotin and ACP showed negligible signals in comparison to those for APE1. Exo III and Endo IV are two prokaryotic analogues of APE1 (24,25). We tested the effects of AVD on their cleavage of AP sites at relatively high enzymatic concentrations. Unlike Endo IV, which showed a lower hydrolytic rate on ACP than P2-biotin, Exo III showed enhanced signals in the presence of AVD, most likely because Exo III belongs to the same family (Class II) as APE1, and the two enzymes have similar folding topology and utilize the same catalytic residues and active center in hydrolyzing the phosphodiester bonds in both the endo- and exonucleolytic cleavage (26–28). Above results indicated that AVD exhibits a chaperone-like property in ACP, making it a promising molecular tool for the specific detection of APE1 in mammalian cells.

To assess the sensitivity of ACP, we measured its response signals to different concentrations of APE1 (Figure 1F). The probe showed a linear working range from 0.002 to 1.0 U/ml of APE1 and a detection limit of 0.0005 U/ml (0.6 pg/ml based on the latest data from NEB) (Figure 1G). This sensitivity was much higher than existing fluorescent probes for the direct detection of APE1 without any additional amplification steps (18,29). More importantly, excellent linear regression results were observed between 0.002 and 0.1 U/ml of APE1 (Figure 1G, inset), which offers a powerful molecular tool to quantify ultra-low levels of APE1 in various cellular samples and exosomes as well.

## *In-vitro* quantification of APE1 activity in subcellular compartments and exosomes of different cell types by using ACP

We used ACP to measure the activity of APE1 in the cytoplasmic and nuclear extracts of several types of cells, including human embryonic kidney cells (HEK-293T), non-cancerous human breast epithelial cells (MCF-10A), human breast adenocarcinoma cells (MCF-7), adenocarcinomic human alveolar basal epithelial cells (A549), human cervical carcinoma cells (HeLa), and pheochromocytoma (PC-12) cells with neuroendocrine cell characteristics. H2B was used as the endogenous references for the nuclear fraction (Supplementary Figure S3A). The recoveries of all the tested protein extracts were in the range of 75–125% (at a spiking level of 0.20 U/ml APE1), which proves the reliability of the measurement results (Figure 2A).

Significant differences in APE1 levels were observed among different cell types (Figure 2A). The cytoplasmic APE1 level in MCF-7 cells was 0.68 ± 0.01 ng/μg protein, only slightly higher than that in the cytoplasm of MCF-10A cells, which was 0.52 ± 0.01 ng/μg protein. In contrast, the nuclear APE1 level in MCF-7 cells was 8.22 ± 0.21 ng/μg protein, which was one order of magnitude higher than that of 0.66 ± 0.08 ng/μg protein in the nucleus of MCF-10A cells. These results are consistent with previously reported data obtained using a DNA/RNA hybrid probe and LC-MS/MS (30,31).

To eliminate the possible interference of other nucleases on the ACP assay, we prepared a control probe (ACP-T) by replacing the AP site with a normal T base. Figure 2B compared the fluorescence responses of ACP and ACP-T to standard APE1 (0.5 U/ml) or diluted nuclear and cytoplasmic extracts (from HeLa cells) containing approximately 0.5 U/ml APE1, respectively. No fluorescent signals were observed when ACP-T was added to the APE1 standard solution. The signals generated by ACP-T in the cytoplasm and nucleus of HeLa cells were less than 4% and 1% of those generated by ACP, respectively.

APE1 is responsible for repairing AP sites in both nucleus and mitochondria. The presence of APE1 inside mitochondria of some tissue or cell types has been demonstrated by Western blot analysis in several studies (32). Here, we extracted mitochondrial proteins and cytosolic proteins from MCF-10A and MCF-7 cells (Supplementary Figure S3B), respectively, and compared the APE1 content in these samples (Figure 2C). For MCF-10A cells, the APE1 level in the mitochondria was 0.084 ± 0.002 ng/μg protein, which was only about 1/8 of that in the cytosol (0.64 ± 0.01 ng/μg protein). Similar results were observed for MCF-7 cells, where the APE1 content in the mitochondria was only about 1/6 of that in the cytosol. It is worth noting that the total amount of APE1 in the mitochondrial and cytosolic fractions was 0.54 ng/μg protein and 0.78 ng/μg protein for MCF-10A and MCF-7, respectively. These values were quite close to the results obtained from cytoplasmic extracts (0.52 ± 0.01 ng/μg protein and 0.68 ± 0.01 ng/μg protein, respectively), demonstrating the good reproducibility of the ACP method.

To further validate the reliability of the ACP assay results, we performed Western blot analysis of cytosolic and mitochondrial protein extracts from MCF-7 and MCF-10A cells, with Actin and COX IV as the normalization markers for the cytosolic and mitochondrial extracts, respectively. As shown in Figure 2D, the results were in good agreement with those obtained by the ACP assay (Figure 2A and C). The mitochondrial APE1 levels were lower than those in the cytosol for both cell types. The cytosolic APE1 level in MCF-7 cells was close to that in MCF-10A cells.

The D210 residue of APE1 plays a critical role in the catalytic reaction, and the D210A mutant showed a 25 000-fold reduction in cleavage activity (33). Figure 2E compared the responses of ACP to wild-type APE1 and APE1 D210A mutant. Mixing ACP with the APE1 D210A mutant did not result in any increase in fluorescence signal, confirming that the sensitive response of ACP to wild-type APE1 is due to the enzyme's specific cleavage at AP sites. To verify that ACP is indeed recognized by APE1 within cells, we sequentially conducted immunoprecipitation and enzyme activity

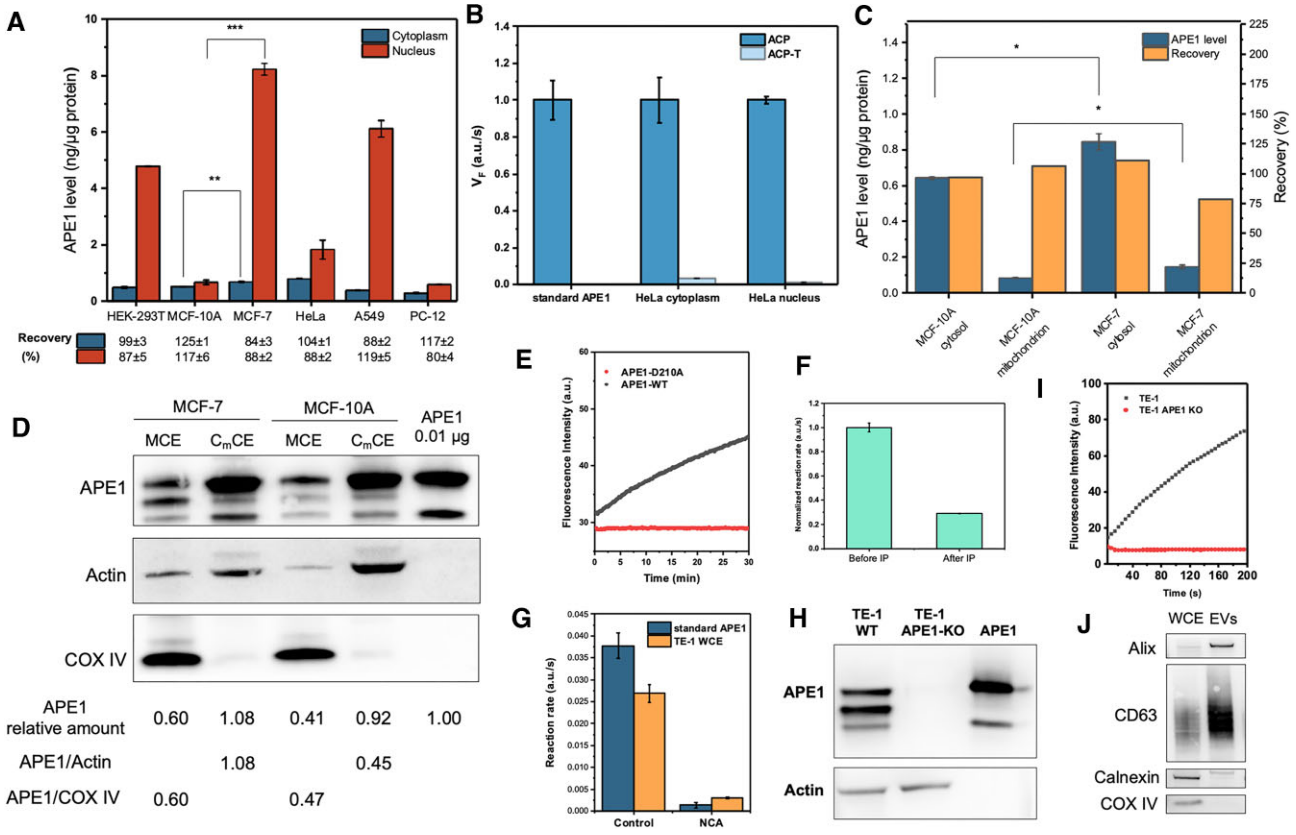


**Figure 2.** (**A**) Quantification of the APE1 level in the cytoplasmic and nuclear extracts of different types of cells by using ACP (** $P \leq 0.01$; *** $P \leq 0.001$). Data showed the mass of APE1 (in ng) per microgram (μg) of total cytoplasmic or nuclear protein. The detailed recovery results for all the tested samples were presented. (**B**) Verification of the measurement results obtained by ACP. Data showed the fluorescent signals of ACP and ACP-T (a control probe in which the AP site was replaced with a normal base T) in response to APE1 standard (0.5 U/ml) and the cytoplasmic extracts and nuclear extracts of HeLa cells, respectively. (**C**) Quantification of the APE1 level in the cytosolic and mitochondrial extracts of MCF-10A and MCF-7 by using ACP (* $P \leq 0.05$). Data showed the mass of APE1 (in ng) per microgram (μg) of total cytosolic or mitochondrial protein. The detailed recovery results for all the tested samples were presented. (**D**) Western blot analysis of APE1 levels in the cytosolic and mitochondrial extracts of MCF-10A and MCF-7. $C_mCE$: cytosolic cell extracts; MCE: mitochondrial cell extracts; Actin and COX IV were used as the normalization markers for the cytosolic and mitochondrial extracts, respectively. (**E**) Comparison of the fluorescence signals of ACP to wild-type APE1 and APE1 D210A mutant. (**F**) Comparison of the responses of ACP before and after immunoprecipitation with APE1 in the cytoplasmic cell extraction of MCF-7 cells. (**G**) Verification of the specificity of ACP using an inhibition test with NCA in the whole cell extracts (WCE) of TE-1 cells. (**H**) Validation of the TE-1 APE1-KO cell lines through Western blotting. (**I**) Comparison of the fluorescence signals of ACP in the WCE of TE-1 WT and TE-1 APE1-KO. (**J**) Verification of the quality of the exosome fraction. The markers for exosomes include Alix and CD63. COX IV and calnexin are the markers of mitochondrial and endoplasmic reticulum, respectively. All experiments were repeated at least three times.

inhibition tests. The IP efficiency of the cytoplasmic cell extracts (CCE) of MCF-7 cells was examined by Western blotting (Supplementary Figure S4). From the results shown in Figure 2F, the fluorescence signal of ACP decreased to less than 30% of its original intensity after immunoprecipitation. 7-nitroindole-2-carboxylic acid (NCA) serves as an APE1-specific inhibitor. We performed inhibition tests with NCA in the whole cell extracts (WCE) of the human esophageal squamous cell carcinoma (TE-1) cell lines. As shown in Figure 2G, upon the addition of NCA, the fluorescence rise rate of ACP in the TE-1 WCE significantly decreased. Although the inhibition efficiencies of NCA on APE1 activity in the TE-1 WCE were not as high as those in the APE1 standard solution due to the interference of cellular proteins, the results confirmed that the fluorescence signals of ACP originated from the cleavage of the AP sites by APE1 in the cell extract samples.

To corroborate the above findings, we further conducted additional comparative experiments utilizing TE-1 wild-type (WT) and TE-1 APE1-knockout (KO) cells. We validated the TE-1 APE1-KO cell lines through Western blotting, confirming the absence of the APE1 protein (Figure 2H). Subsequently, we measured the APE1 content in the WCE of TE-1 WT and TE-1 APE1-KO using ACP. As illustrated in Figure 2I, the fluorescence signal of ACP increased rapidly in the TE-1 WT WCE, whereas in the TE-1 APE1-KO WCE, ACP showed almost no response. These results substantiated that the fluorescence signals observed with ACP in cell lysates resulted from the cleavage of AP sites in ACP by APE1.

As a non-classical secretory protein, APE1 has been found to be secreted through extracellular vesicles, especially exosomes (34,35). We quantified the level of APE1 in the exosomes from A549 cells using ACP, which was determined to be $0.05 \pm 0.01$ ng/μg protein, approximately 1/8 and 1/136 of the APE1 content in the cytoplasm and nucleus, respectively. We also measured the level of APE1 in the exosomes from PC-12 cells using ACP. The quality of the exosome fraction was verified by the mitochondrial marker COX IV and the endoplasmic reticulum marker calnexin (Figure 2J). The markers for exosomes included Alix and CD63. The relative abundance of APE1 in exosome and different organelles of

PC-12 cells was observed to be in following order (ng/μg protein): exosome (0.004 ± 0.001) ≈ mitochondria (0.004 ± 0.001) < cytosol (0.07 ± 0.01) < nucleus (0.16 ± 0.01). The secretion of APE1 through exosomes from cancer cells may play important roles in tumor progression (36), as exosomes are known to have various functions in intercellular communication. The ACP assay may facilitate the quantitative investigations on the correlation between the tumor stages and the APE1 level in exosomes and putative subcellular compartments.

Compared to existing approaches, the LC–MS/MS method required approximately $3 \times 10^7$ cells per sample, and the sample pre-treatment process was time-consuming and labor-intensive, with no spike-recovery data reported (30). In contrast, the ACP only needed a few hundred cells, and no additional sample purification or enrichment steps were required. In comparison with previously reported APE1 nanoprobes (9), ACP demonstrates several advantageous features as a single-molecular complex. These include a smaller size, enhanced dispersibility, improved biocompatibility and increased potential for various intracellular applications.

## Modification of ACP with phenylboronic acid for nucleus targeted delivery

Phenylboronic acid modification has been reported as an effective non-peptide approach to assist in the translocation of several proteins from the cytoplasm into the nucleus via the importin α/β pathway (37). Different from previously reported proteins that have been modified with phenylboronic acid for nucleus-targeted translocation, AVD bears glycosyl residues that may also react with boronic acid and form cyclic borate ester linkages. We synthesized 4-nitrophenyl 4-(4,4,5,5-tetramethyl-1,3,2-dioxaborolan-2-yl)benzyl carbonate (PBN) (Supplementary Figure S5) and conjugated the phenylboronate ester to the lysine residues on AVD through a covalent carbamate linker (Scheme 1B). In aqueous solutions, the phenylboronate ester was quickly hydrolyzed into aryl boronic acid. The phenylboronic acid-modified AVD (denoted as PB-AVD) was characterized using matrix-assisted laser desorption/ionization with time-of-flight mass spectrometry (MALDI-TOF MS). The MALDI spectra of AVD and PB-AVD (Figure 3A) both showed the four peaks corresponding to monomer, dimer, trimer, and tetramer, respectively. In comparison with unreacted AVD, PB-AVD showed a 389.71 Da increase per monomer, a 997.41 Da increase per dimer, a 1157.58 Da increase per trimer, and a 2372.10 Da increase per tetramer, respectively. The average increase per subunit was calculated to be 389.71, 498.70, 578.79, and 593.02, respectively, suggesting that the labeling ratio of PB on each subunit was about 2–3. From the increase in the relative intensity of dimer, trimer, and tetramer compared to the monomer intensity in PB-AVD (Figure 3A), only a few AVD molecules were crosslinked via borate ester linkages. The monomers and dimers were the predominant species, indicating that most of the labeled phenylboronic acid groups were exposed to the solution. Supplementary Figure S6 compared the rates of fluorescence signal rise generated by digestion of PB-ACP by APE1 (1.0 U/ml, 32.9 pM), DNase I (1.0 U/ml, 685 pM) and TREX1 (55 nM), which confirmed the high selectivity of PB-ACP toward APE1.

Next, we attempted to deliver the obtained PB-ACP into the nucleus of living cells as shown in Scheme 1C. PC-12 cell has been widely used as a model of neuron cells (38,39). Figure 3B showed the representative images of PC-12 cells acquired at 0, 1, 2, 3, 4 and 5 h after transfection of PB-ACP with Lipofectamine 3000 Reagent. Continuous enhancement of fluorescence intensity within the nucleus of PC-12 cells were clearly observed (Supplementary Figure S7), indicating that PB-ACP could be efficiently internalized by PC-12 cells in the presence of liposomes and then rapidly enter the nucleus. Due to the highly efficient transportation of PB-ACP into the nucleus, and much higher level of APE1 in the nucleus than in cytoplasm, the fluorescence signals within the nucleus were significantly brighter than those in the cytoplasmic region. As the increase of the fluorescence intensity gradually slowed down after 4 h, the fluorescence images in subsequent experiments were all acquired at 4 h after PB-ACP were transfected. To confirm the results of the intracellular signals of APE1 obtained by PB-ACP, we further performed comparison experiments using a control probe (PB-ACP-T) in which a normal T base was substituted for the AP site. As shown in Figure 3C and Supplementary Figure S8, the fluorescent signals generated by PB-ACP-T were negligible compared to those obtained by PB-ACP under the same experimental conditions, which proved that the fluorescence signals of PB-ACP in the nucleus of PC-12 living cells originated from the cleavage of the AP sites in PB-ACP by APE1.

Following the results in Figure 2I, we conducted further fluorescence imaging on live TE-1 WT and TE-1 APE1-KO cells using PB-ACP (Figure 3E-G). It was evident that PB-ACP efficiently entered the cell nucleus and emitted bright fluorescence in TE-1 WT cells. In contrast, minimal fluorescence resulting from enzymatic hydrolysis was observed within the cells of TE-1 APE1-KO. These findings provided additional support for the reliability of PB-ACP.

To verify the contribution of PB modification to the nucleus-targeted delivery of ACP in PC-12 cells, we performed a comparative study with ACP and PB-ACP under the same experimental conditions. As shown in Supplementary Figure S9, for ACP without PB modification, after transfection with liposomes, the fluorescent signals were mainly distributed near the cell membrane. Whereas for PB-ACP, the quick diffusion of the fluorescent signals in the cytoplasmic region and subsequent accumulation inside the nucleus could be clearly observed. We also tested incubation of PB-ACP with PC-12 cells in the absence of liposomes; no fluorescence signals were observed either in the cytoplasm or in the nucleus. These results proved that liposomes played an important role in transfecting PB-ACP into the cytoplasm of living cells, while PB modification enabled subsequent translocation of the probes into the nucleus.

## Visualization of the distribution of APE1 within the nucleus and nucleolus

The nucleolus is the largest subnuclear organelle in eukaryotic cells. It is membrane-free and mainly composed of rRNA, rDNA, and various proteins. Through immunofluorescence or fluorescent fusion proteins, several studies have suggested that APE1 accumulates in the nucleolus (40–42). However, the actual distribution of endogenous APE1 in the nucleus and nucleolus of living cells remains unexplored.

We incubated live PC-12 cells with both PB-ACP and Hoechst 33342 and obtained magnified cellular fluorescence images (Figure 4A–D). Figures 4E and F respectively depicted

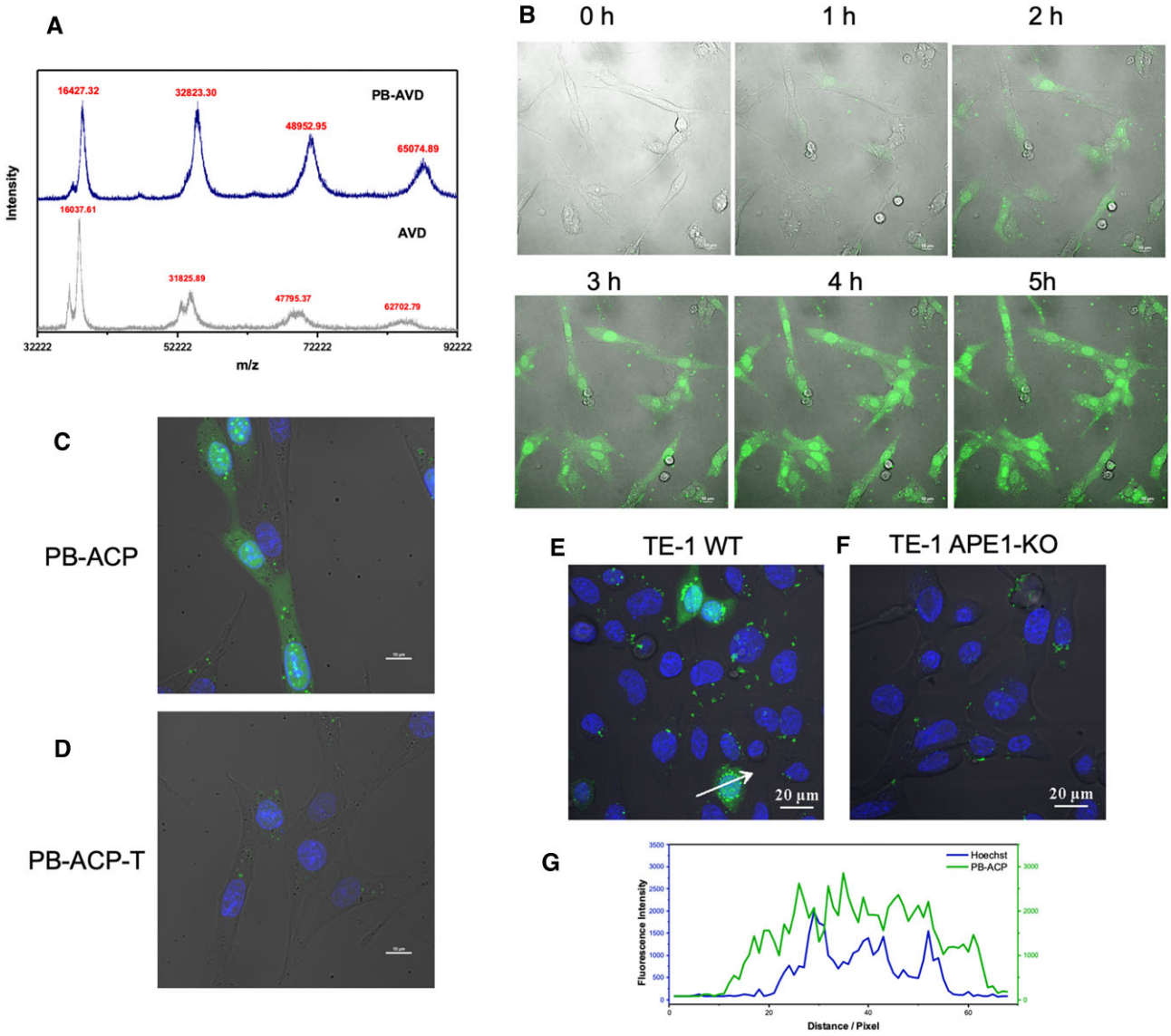


**Figure 3.** (**A**) MALDI-TOF mass spectra of AVD and PB-AVD. (**B**) Time-lapse fluorescence imaging of the activity of APE1 (green) in the nucleus of PC-12 living cells by using PB-ACP. (C, D) Comparison of the fluorescent images of APE1 activity (green) in PC-12 living cells obtained by using PB-ACP (**C**) and PB-ACP-T (**D**), respectively. PB-ACP-T is a control probe in which the AP site is replaced with a normal base T. Hoechst 33342 was used to stain the nucleus (blue). (E, F) Fluorescence imaging of live TE-1 WT (**E**) and TE-1 APE1-KO (**F**) cells using PB-ACP. (**G**) Fluorescence profiles along the white solid arrow drawn across the representative cell in (E).

the results of Hoechst 33342 staining and the distribution of PB-ACP fluorescence signals within the same cell (marked with a red box). Significant differences could be observed between the two images. In regions where Hoechst 33342 fluorescence was relatively weak, brighter PB-ACP fluorescence signals were observed. Figures 4H and I displayed the magnified images of another cell within the same field of view (marked with a white box). Similarly, in the more loosely organized, transcriptionally active euchromatin and the nucleolus, which were lightly stained with Hoechst 33342, PB-ACP exhibited stronger fluorescence signals. Figure 4G represented the plot of intensity values along the red arrow drawn across the cell in Figures 4E and F, where the positions with the strongest PB-ACP signals corresponded to lower DNA content. In Figure 4J, the plot of intensity values along the white arrow drawn across the cell in Figures 4H and I also revealed multiple positions with higher PB-ACP fluorescence signals, accompanied by a decrease in Hoechst 33342 signals. In the more densely packed heterochromatin region that was strongly stained with Hoechst 33342, the signals of PB-ACP were of moderate intensity. These results suggested that APE1 was more abundantly distributed in the nucleolus or euchromatin regions.

In addition to PC-12 cells, we also performed imaging on live HEK-293T cells using PB-ACP (Figure 4K–M and Supplementary Figure S10). The subcellular localization of APE1 in the nucleus of HEK-293T cells was similar to that in PC-12 cells, showing multiple regions where PB-ACP signals reached peak values, while the Hoechst 33342 signal was relatively low. In Figure 3G, we have included the fluorescence profiles along the white solid arrow drawn across a TE-1 WT cell from Figure 3E, which revealed a general negative correlation between the fluorescence signals of PB-ACP and the Hoechst 33342 signals.

To further inspect the distribution of APE1 within the nucleus, we attempted to stain the nucleolus with acridine orange

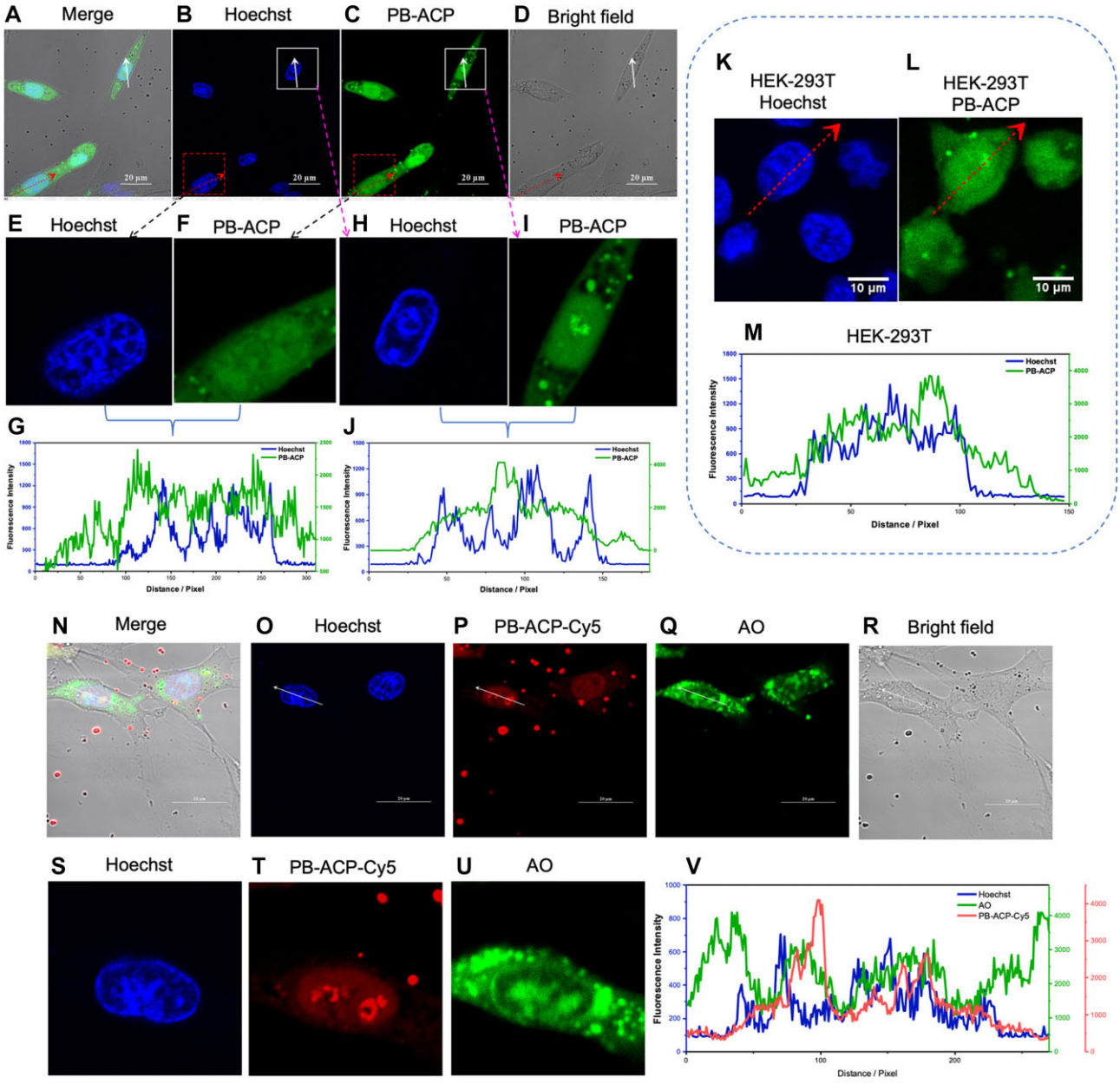


**Figure 4.** (**A–D**) Visualization of APE1 activity (green) in the nucleus of PC-12 living cells using PB-ACP. Hoechst 33342 was used to stain the nucleus (blue). (**E**) The magnified image of the cell marked with a red box in (B). (**F**) The magnified image of the cell marked with a red box in (C). (**G**) Fluorescence profiles along the red arrow drawn across the cell marked with a red box in (B). (**H**) The magnified image of the cell marked with a white box in (B). (**I**) The magnified image of the cell marked with a white box in (C). (**J**) Fluorescence profiles along the white arrow drawn across the cell marked with a white box in (B). (**K, L**) Visualization of APE1 activity (green) in the nucleus of HEK-293T cells using PB-ACP. Hoechst 33342 was used to stain the nucleus (blue). (**M**) Fluorescence profiles along the red arrow drawn across the representative cell in (K and L). (**N–R**) Visualization of APE1 activity in the nucleus and nucleolus of PC-12 living cells using PB-ACP-Cy5 (red) and AO (green). Hoechst 33342 was used to stain the nucleus (blue). (**S–U**) The magnified images of the cell marked with a white arrow in (O), (P) and (Q), respectively. (**V**) Fluorescence profiles along the white arrow drawn across the representative cell in (O–Q).

(AO), which binds to RNA with enhanced fluorescence intensity. However, AO also embeds itself between base pairs in the DNA duplex, which may affect the cleavage of PB-ACP by APE1 (43). From the fluorescence images of cells stained with different concentrations of AO (Supplementary Figure S11), when the concentration of AO was greater than or equal to 0.5 μg/ml, we could clearly distinguish the location of the nucleolus from the fluorescence image. Supplementary Figure S12 showed that as the concentration of AO increased, the cleavage rate of ACP by APE1 notably decreased. At an AO concentration of 1.0 μg/ml, the response rate of ACP to APE1 decreased by about 50%. Based on these results, we used AO dye at a final concentration of 0.5 μg/ml. To avoid the spectral overlap of the probe signal caused by the wider fluorescence emission interval of the AO dye, we prepared PB-ACP-Cy5 by replacing FAM and BHQ1 in PB-ACP with Cy5 and BHQ2, respectively.

PC-12 cells were sequentially incubated with PB-ACP-Cy5, Hoechst 33342 nucleus dye, and AO nucleolus dye. The results were presented in Figure 4N–R. The magnified images

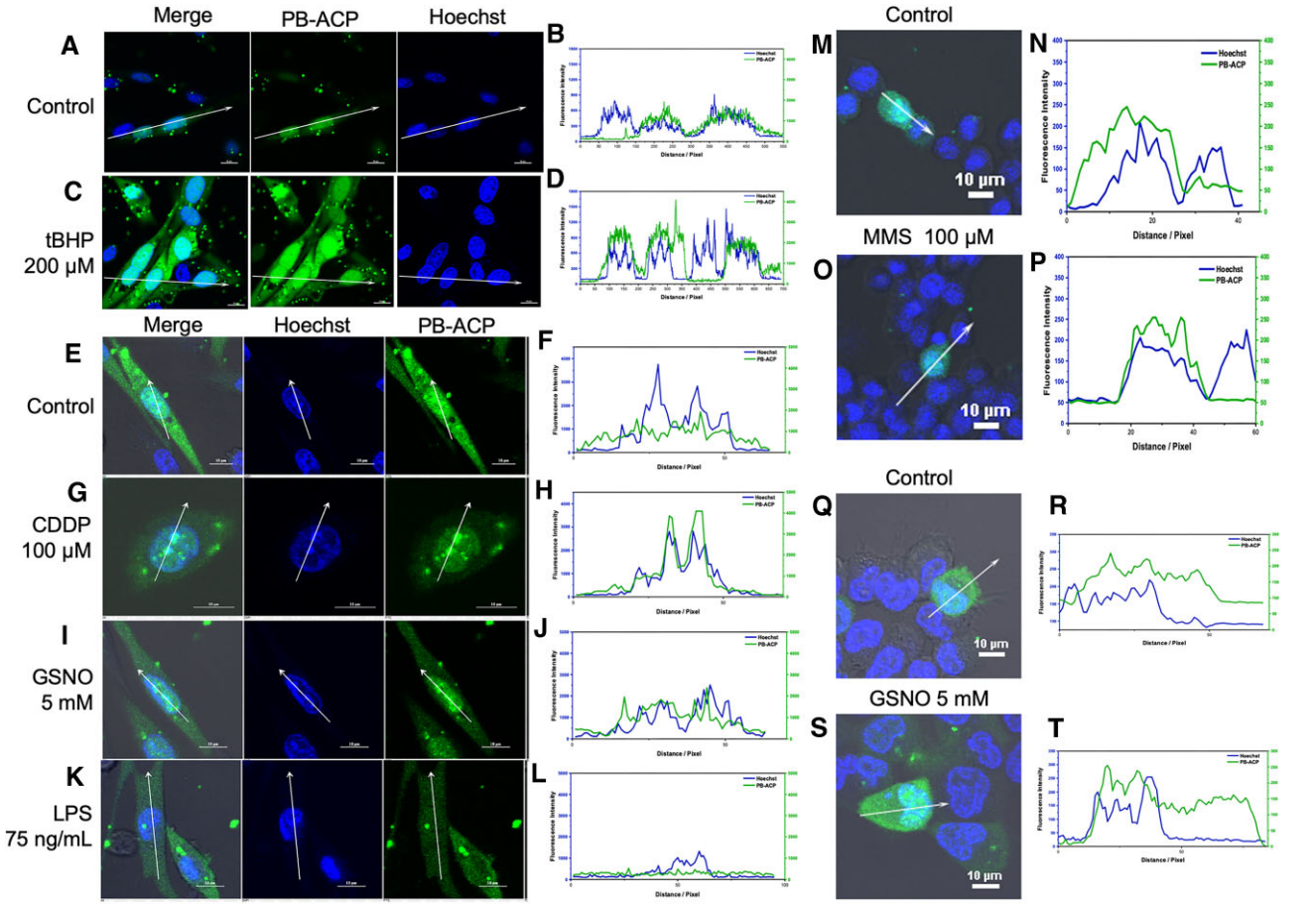


**Figure 5.** Visualization of the activity and distribution of APE1 (green) within the nucleus of PC-12 or HEK-293T living cells under various treatment by using PB-ACP. Hoechst 33342 was used to stain the nucleus (blue). (**A**) APE1 in the nucleus of untreated PC-12 living cells (Control for (B)). (**B**) Fluorescence profiles along the white arrow drawn across the representative cells in (A). (**C**) APE1 in the nucleus of PC-12 living cells treated with tBHP (200 μM). (**D**) Fluorescence profiles along the representative cells in (C). (**E**) APE1 in the nucleus of untreated PC-12 living cells (Control for (G, I, K)). (**F**) Fluorescence profiles along the marked cell in (E). (**G**) APE1 in the nucleus of PC-12 living cells treated with CDDP (100 μM). (**H**) Fluorescence profiles along the marked cell in (G). (**I**) APE1 in the nucleus of PC-12 living cells treated with GSNO (5 mM). (**J**) Fluorescence profiles along the marked cell in (I). (I) APE1 in the nucleus of PC-12 living cells treated with GSNO (5 mM). (J) Fluorescence profiles along the marked cell in (I). (**K**) APE1 in the nucleus of PC-12 living cells treated with LPS (75 ng/ml). (**L**) Fluorescence profiles along the marked cell in (K). (**M**) APE1 in the nucleus of untreated PC-12 living cells (Control for (O)). (**N**) Fluorescence profiles along the marked cell in (M). (**O**) APE1 in the nucleus of PC-12 living cells treated with MMS (100 μM). (**P**) Fluorescence profiles along the marked cell in (O). (**Q**) APE1 in the nucleus of untreated HEK-293T living cells. (**R**) Fluorescence profiles along the marked cell in (Q). (**S**) APE1 in the nucleus of HEK-293T living cells treated with GSNO (5 mM). (**T**) Fluorescence profiles along the marked cell in (S).

of a representative cell were displayed in Figure 4O–Q. The distribution of the fluorescence signals of PB-ACP-Cy5 and Hoechst 33342 was generally consistent with the results in Figure 4A–I obtained without AO. From the intensity value plots of a line drawn across the cell shown in Figure 4V, most regions with strong AO signals within the cell nucleus also exhibited intense signals of PB-ACP-Cy5, providing evidence for APE1's distribution within the nucleolus. This represents the first observation of native APE1 in the nucleolus of living cells.

APE1 plays distinct roles in different cellular regions. Its main functions include RNA regulation in the nucleolus and endonuclease activity in euchromatin and heterochromatin. In regions of euchromatin with active gene expression and a higher degree of DNA damage, a greater amount of APE1 is required to participate in repair processes and maintain genome stability. The elevated level of APE1 in the euchromatin region may indicate its involvement in the BER pathway. APE1's extensive distribution throughout the cell nucleus also suggests its dynamic translocation to perform diverse functions.

## Monitoring of the dynamics of nuclear APE1 under various stimulation treatments

APE1 plays an important role in repairing DNA damage caused by oxidative agents. tBHP is a strong oxidative stress-inducing agent commonly used to induce the production of reactive oxygen species (ROS) in cells (44). To visualize changes in APE1 within the nucleus of living cells under oxidative stress, we first tested the effect of different concentrations of tBHP (25-400 μM) on ROS production in PC-12 cells. From Supplementary Figure S13, we observed weak fluorescent signals, indicating the presence of ROS in some cells when the tBHP concentration increased from 25 to 100 μM. When the tBHP concentration reached 200 μM and above, green fluorescence signals could be observed in almost all cells, indicating significantly enhanced ROS levels. Accordingly, we used 200 μM tBHP to monitor the response of PC-12 cells in its APE1 level to the oxidative stimulation.

Under the treatment of 200 μM tBHP, the fluorescence intensity of PB-ACP significantly enhanced (Figure 5C) in contrast to the control group (Figure 5A), indicating substan-

tially elevated intracellular level of APE1, especially inside the nucleus. Figure 5C showed an overall increase in fluorescence intensity inside the nucleus, with very strong signals in the nucleolus and euchromatin regions. Compared to the untreated cells, the average fluorescence intensity increased to 1.9-fold in the nucleus of the tBHP-stimulated cells (Supplementary Figure S14). These results indicated that PB-ACP could be used to trace the variation of APE1 in nucleus.

To further confirm the reliability of above fluorescence imaging results, we stimulated PC-12 cells using the same condition of tBHP, and then lysed the cells and collected protein extracts from the nucleus. The APE1 level in the cell extracts was quantitatively measured using ACP. Supplementary Figure S15 showed that the APE1 level in the nucleus of tBHP-treated cells increased by about 1.8-fold as high as those untreated cells, which was generally consistent with that observed in the living cells by fluorescence imaging.

Next, we further explored the changes of APE1 within the nuclei of PC-12 living cells under additional stimulation treatments, with results summarized in Figures 5E–L and Supplementary Figure S16. *cis*-Diamminedichloroplatinum (CDDP) is a chemotherapy drug employed in treating various cancers (45). It acts, in part, by binding to DNA and impeding its replication. Upon treatment with 100 μM CDDP (Figures 5G and H), APE1 within the PC-12 cell nucleus tended to aggregate in regions of higher DNA density, where the fluorescence intensity of PB-ACP was notably higher than in neighboring regions with weak Hoechst 33342 signals. This change may be associated with the relocation of APE1 from the nucleolus to the chromatin. S-nitrosoglutathion (GSNO) is a widely used S-nitrosating agent (46). After treating PC-12 cells with 5 mM GSNO (Figures 5I and J), APE1 distribution within the nucleus remained uneven, with fluorescence signals observed in regions of both high and low DNA content. However, in some areas with weak Hoechst 33342 signals, APE1 signals appeared more concentrated and brighter.

Lipopolysaccharides (LPS), also known as endotoxin, are potent activators of the immune system (47,48). Following LPS treatment (75 ng/ml) (Figure 5K and L), there was a significant decrease in fluorescence intensity of PB-ACP throughout the entire cell nucleus, suggesting a potential export of APE1 from the nucleus to the cytoplasm.

Methyl methanesulfonate (MMS) is an alkylating agent and a carcinogenic toxicant (49). We also subjected PC-12 living cells to MMS treatment. As shown in Figures 5M to P and Supplementary Figure S17, after 2 h treatment with 100 μM MMS, there was not a substantial change in the distribution of APE1 within the cell nucleus. In some regions with weak Hoechst 33342 signals, strong APE1 signals were still evident. We attempted the use of a higher concentration of MMS, but observed morphological abnormalities in PC-12 cells, including the appearance of numerous dead cells.

We also extended our observations to HEK-293T living cells using PB-ACP after treating the cells with 5 mM GSNO for 2 h (Figures 5Q to T and Supplementary Figure S18). In comparison to the control group, APE1 signals appeared more concentrated and brighter in some regions with weak Hoechst 33342 signals. Further exploration of the detailed changes and response mechanisms is ongoing and will be reported in subsequent studies.

By utilizing PB-AVD as a chaperone, the developed PB-ACP ensures specificity without requiring any chemical modification of the DNA backbone. This innovative approach enables the in-situ tracking of APE1 activity variation in the nucleus of living cells with good biocompatibility and stability. The method opens up opportunities to monitor the distinct responses between normal and cancerous living cells regarding nuclear APE1 activity under external treatment conditions (50). Comparing the differences in repair processes between normal and cancer cells may facilitate the identification of appropriate time windows or doses for more precise and effective treatments.

## Conclusions

In this work, we have demonstrated a novel chaperone@DNA molecular tool, the phenylboronic acid modified avidin conjugated abasic site-containing DNA probe (PB-ACP), for direct observation of APE1 in the nucleus in living cells. The phenylboronic acid modified avidin not only serves as a chaperone to protect the AP-DNA from being nonspecifically degraded, but also facilitates nucleus targeted delivery of the probe. The PB-ACP shows high specificity and sensitivity to APE1 due to the strong binding affinity of APE1 to both avidin and the AP site in DNA. The probe can efficiently migrate from cytoplasm to the nucleus and specifically display the distribution and in-vivo activity of endogenous nuclear APE1. It offers a powerful tool to investigate the cellular behavior of APE1 in living cells and to improve cancer therapies targeting APE1.

## Data availability

The data supporting the findings of this study are available within the paper and its Supplementary Information, and additional data are available from the corresponding author on reasonable request.

## Supplementary data

Supplementary Data are available at NAR Online.

## Acknowledgements

We thank the Analytical Instrumentation Center in Peking University (PKUAIC) for assistance with the MALDI-TOF MS analysis and Optical Spectroscopy measurement. We thank Dr Wen Zhou at PKUAIC for the help with the MALDI-TOF MS analysis and Dr Yan Guan at PKUAIC for the help with Optical Spectroscopy measurement.

*Author contributions:* X.C. and M.Z. designed research; X.C., J.Z., R.Z. and Y.S. performed research; X.C., J.Z. and M.Z. analyzed data; X.C. and M.Z. wrote the paper.

## Funding

National Natural Science Foundation of China [21974005, 22174005, 22374002]. Funding for open access charge: National Natural Science Foundation of China.

## Conflict of interest statement

Peking University has filed a patent application on the technologies described herein.

## References


1. Mijit,M., Caston,R., Gampala,S., Fishel,M.L., Fehrenbacher,J. and Kelley,M.R. (2021) APE1/Ref-1 - one target with multiple indications: emerging aspects and new directions. *J. Cell. Signal.*, **2**, 151–161.
2. Evans,A.R., Limp-Foster,M. and Kelley,M.R. (2000) Going APE over ref-1. *Mutat. Res. DNA Repair*, **461**, 83–108.
3. Shah,F., Logsdon,D., Messmann,R.A., Fehrenbacher,J.C., Fishel,M.L. and Kelley,M.R. (2017) Exploiting the ref-1-APE1 node in cancer signaling and other diseases: from bench to clinic. *Npj Precis. Oncol.*, **1**, 19.
4. Demple,B., Herman,T. and Chen,D.S. (1991) Cloning and expression of APE, the cDNA encoding the major human apurinic endonuclease: definition of a family of DNA repair enzymes. *Proc. Natl. Acad. Sci. U.S.A.*, **88**, 11450–11454.
5. Fishel,M.L. and Kelley,M.R. (2007) The DNA base excision repair protein Ape1/ref-1 as a therapeutic and chemopreventive target. *Mol. Aspects Med.*, **28**, 375–395.
6. Barnes,T., Kim,W.C., Mantha,A.K., Kim,S.E., Izumi,T., Mitra,S. and Lee,C.H. (2009) Identification of Apurinic/apyrimidinic endonuclease 1 (APE1) as the endoribonuclease that cleaves c-myc mRNA. *Nucleic Acids Res.*, **37**, 3946–3958.
7. Kelley,M.R., Logsdon,D. and Fishel,M.L. (2014) Targeting DNA repair pathways for cancer treatment: what's new?*Future Oncol.*, **10**, 1215–1237.
8. Di Maso,V., Mediavilla,M.G., Vascotto,C., Lupo,F., Baccarani,U., Avellini,C., Tell,G., Tiribelli,C. and Croce,L.S. (2015) Transcriptional up-regulation of APE1/ref-1 in hepatic tumor: role in hepatocytes resistance to oxidative stress and apoptosis. *PLoS One*, **10**, e0143289.
9. Zhai,J.Q., Liu,Y.B., Huang,S., Fang,S.M. and Zhao,M.P. (2017) A specific DNA-nanoprobe for tracking the activities of human apurinic/apyrimidinic endonuclease 1 in living cells. *Nucleic Acids Res.*, **45**, e45.
10. Lv,M.M., Liu,J.W., Yu,R.Q. and Jiang,J.H. (2020) A bipedal DNA nanowalker fueled by catalytic assembly for imaging of base-excision repairing in living cells. *Chem. Sci.*, **11**, 10361–10366.
11. Lu,P., Cao,X., Zheng,J., Sun,Y., Tang,Z. and Zhao,M. (2023) Visualization and comparison of the level of apurinic/apyrimidinic endonuclease 1 in live normal/cancerous and neuron cells with a fluorescent nanoprobe. *Molecules*, **28**, 3935.
12. Ramana,C.V., Boldogh,I., Izumi,T. and Mitra,S. (1998) Activation of apurinic/apyrimidinic endonuclease in human cells by reactive oxygen species and its correlation with their adaptive response to genotoxicity of free radicals. *P.roc Natl. Acad. Sci. U.S.A.*, **95**, 5061–5066.
13. Tell,G., Di Piazza,M., Kamocka,M.M. and Vascotto,C. (2013) Combining RNAi and in vivo confocal microscopy analysis of the photoconvertible fluorescent protein Dendra2 to study a DNA repair protein. *BioTechniques*, **55**, 198–203.
14. Lee,Y.R., Lim,J.S., Shin,J.H., Choi,S., Joo,H.K. and Jeon,B.H. (2016) Altered secretory activity of APE1/ref-1 D148E variants identified in Human patients with bladder cancer. *Int. Neurourol. J.*, **20**, S30–S37.
15. Janoshazi,A.K., Horton,J.K., Zhao,M.L., Prasad,R., Scappini,E.L., Tucker,C.J. and Wilson,S.H. (2020) Shining light on the response to repair intermediates in DNA of living cells. *DNA Repair (Amst.)*, **85**, 102749.
16. Brewer,L.R., Corzett,M. and Balhorn,R. (1999) Protamine-induced condensation and decondensation of the same DNA molecule. *Science*, **286**, 120–123.
17. Morpurgo,M., Radu,A., Bayer,E.A. and Wilchek,M. (2004) DNA condensation by high-affinity interaction with avidin. *J. Mol. Recognit.*, **17**, 558–566.
18. Fang,S., Chen,L. and Zhao,M. (2015) Unimolecular chemically modified DNA fluorescent probe for one-step quantitative measurement of the activity of Human apurinic/apyrimidinic endonuclease 1 in biological samples. *Anal. Chem.*, **87**, 11952–11956.
19. Lu,P., Cao,X., Zheng,J., Zhu,C., Zhang,R., Sun,Y., Yang,Z., Tang,Z., Wang,J. and Zhao,M. (2023) A DNA/RNA hybrid fluorescent probe for high-throughput quantification of the activity of human apurinic/apyrimidinic endonuclease 1 in subcellular extracts. *Biosens. Bioelectron. X*, **14**, 100329.
20. Weaver,T.M., Hoitsma,N.M., Spencer,J.J., Gakhar,L., Schnicker,N.J. and Freudenthal,B.D. (2022) Structural basis for APE1 processing DNA damage in the nucleosome. *Nat. Commun.*, **13**, 5390.
21. Livnah,O., Bayer,E.A., Wilchek,M. and Sussman,J.L. (1993) Three-dimensional structures of avidin and the avidin-biotin complex. *Proc. Natl. Acad. Sci. U.S.A.*, **90**, 5076–5080.
22. Ellison,D., Hinton,J., Hubbard,S.J. and Beynon,R.J. (1995) Limited proteolysis of native proteins - the interaction between avidin and proteinase-K. *Protein Sci.*, **4**, 1337–1345.
23. Mazur,D.J. and Perrino,F.W. (1999) Identification and expression of the TREX1 and TREX2 cDNA sequences encoding mammalian 3'→5' exonucleases. *J. Biol. Chem.*, **274**, 19655–19660.
24. Mol,C.D., Hosfield,D.J. and Tainer,J.A. (2000) Abasic site recognition by two apurinic/apyrimidinic endonuclease families in DNA base excision repair: the 3′ ends justify the means. *Mutat. Res./DNA Repair*, **460**, 211–229.
25. Puri,R.V., Singh,N., Gupta,R.K. and Tyagi,A.K. (2013) Endonuclease IV is the major apurinic/apyrimidinic endonuclease in mycobacterium tuberculosis and is important for protection against oxidative damage. *PLoS One*, **8**, e71535.
26. Freudenthal,B.D., Beard,W.A., Cuneo,M.J., Dyrkheeva,N.S. and Wilson,S.H. (2015) Capturing snapshots of APE1 processing DNA damage. *Nat. Struct. Mol. Biol.*, **22**, 924–931.
27. Whitaker,A.M., Flynn,T.S. and Freudenthal,B.D. (2018) Molecular snapshots of APE1 proofreading mismatches and removing DNA damage. *Nat. Commun.*, **9**, 399.
28. Liu,T.-C., Lin,C.-T., Chang,K.-C., Guo,K.-W., Wang,S., Chu,J.-W. and Hsiao,Y.-Y. (2021) APE1 distinguishes DNA substrates in exonucleolytic cleavage by induced space-filling. *Nat. Commun.*, **12**, 601.
29. Wang,J.Y. and Zhao,M.P. (2019) Fluorescence assay for the detection of apurinic/apyrimidinic endonuclease 1 (APE1) activity in human blood samples. *Beijing Da Xue Xue Bao Yi Xue Ban*, **51**, 487–492.
30. Kirkali,G., Jaruga,P., Reddy,P.T., Tona,A., Nelson,B.C., Li,M., Wilson,D.M. 3rd and Dizdaroglu,M. (2013) Identification and quantification of DNA repair protein apurinic/apyrimidinic endonuclease 1 (APE1) in human cells by liquid chromatography/isotope-dilution tandem mass spectrometry. *PLoS One*, **8**, e69894.
31. Coskun,E., Jaruga,P., Reddy,P.T. and Dizdaroglu,M. (2015) Extreme expression of DNA repair protein apurinic/apyrimidinic endonuclease 1 (APE1) in Human breast cancer As measured by liquid chromatography and isotope dilution tandem mass spectrometry. *Biochemistry-US*, **54**, 5787–5790.
32. Bazzani,V., Barchiesi,A., Radecka,D., Pravisani,R., Guadagno,A., Di Loreto,C., Baccarani,U. and Vascotto,C. (2020) Mitochondrial apurinic/apyrimidinic endonuclease 1 enhances mtDNA repair contributing to cell proliferation and mitochondrial integrity in early stages of hepatocellular carcinoma. *BMC Cancer*, **20**, 969.
33. Erzberger,J.P. and Wilson,D.M. (1999) The role of Mg2+ and specific amino acid residues in the catalytic reaction of the major human abasic endonuclease: new insights from EDTA-resistant incision of acyclic abasic site analogs and site-directed mutagenesis. *J. Mol. Biol.*, **290**, 447–457.
34. Lirussi,L., Antoniali,G., Scognamiglio,P.L., Marasco,D., Dalla,E., D'Ambrosio,C., Arena,S., Scaloni,A. and Tell,G. (2020) Cleavage of the APE1 N-terminal domain in acute myeloid leukemia cells is associated with proteasomal activity. *Biomolecules*, **10**, 531.
35. Meisenberg,C., Tait,P.S., Dianova,I.I., Wright,K., Edelmann,M.J., Ternette,N., Tasaki,T., Kessler,B.M., Parsons,J.L., Kwon,Y.T, *et al.*

(2012) Ubiquitin ligase UBR3 regulates cellular levels of the essential DNA repair protein APE1 and is required for genome stability. *Nucleic Acids Res.*, **40**, 701–711.
36. Mangiapane,G., Parolini,I., Conte,K., Malfatti,M.C., Corsi,J., Sanchez,M., Pietrantoni,A., D'Agostino,V.G. and Tell,G. (2021) Enzymatically active apurinic/apyrimidinic endodeoxyribonuclease 1 is released by mammalian cells through exosomes. *J. Biol. Chem.*, **296**, 100569.
37. Tang,R., Wang,M., Ray,M., Jiang,Y., Jiang,Z.W., Xu,Q.B. and Rotello,V.M. (2017) Active targeting of the nucleus using nonpeptidic boronate tags. *J. Am. Chem. Soc.*, **139**, 8547–8551.
38. Hu,R., Cao,Q., Sun,Z., Chen,J., Zheng,Q. and Xiao,F. (2018) A novel method of neural differentiation of PC12 cells by using Opti-MEM as a basic induction medium. *Int. J. Mol. Med.*, **41**, 195–201.
39. Greene,L.A. and Tischler,A.S. (1976) Establishment of a noradrenergic clonal line of rat adrenal pheochromocytoma cells which respond to nerve growth factor. *Proc. Natl. Acad. Sci. U.S.A.*, **73**, 2424–2428.
40. Vascotto,C., Fantini,D., Romanello,M., Cesaratto,L., Deganuto,M., Leonardi,A., Radicella,J.P., Kelley,M.R., D'Ambrosio,C., Scaloni,A., *et al.* (2009) APE1/Ref-1 interacts with NPM1 within nucleoli and plays a role in the rRNA quality control process. *Mol. Cell. Biol.*, **29**, 1834–1854.
41. Lirussi,L., Antoniali,G., Vascotto,C., D'Ambrosio,C., Poletto,M., Romanello,M., Marasco,D., Leone,M., Quadrifoglio,F., Bhakat,K.K., *et al.* (2012) Nucleolar accumulation of APE1 depends on charged lysine residues that undergo acetylation upon genotoxic stress and modulate its BER activity in cells. *Mol. Biol. Cell*, **23**, 4079–4096.
42. Scott,D.D. and Oeffinger,M. (2016) Nucleolin and nucleophosmin: nucleolar proteins with multiple functions in DNA repair. *Biochem. Cell. Biol.*, **94**, 419–432.
43. Mcmaster,G.K. and Carmichael,G.G. (1977) Analysis of single-stranded and double-stranded nucleic-acids on polyacrylamide and agarose gels by using glyoxal and acridine-orange. *Proc. Natl. Acad. Sci. U.S.A.*, **74**, 4835–4838.
44. Zhao,W.W., Feng,H.T., Sun,W., Liu,K., Lu,J.J. and Chen,X.P. (2017) Tert-butyl hydroperoxide (t-BHP) induced apoptosis and necroptosis in endothelial cells: roles of NOX4 and mitochondrion. *Redox. Biol.*, **11**, 524–534.
45. Pan,S.T., Zhou,J., Yang,F., Zhou,S.F. and Ren,T. (2020) Proteomics reveals a therapeutic vulnerability via the combined blockade of APE1 and autophagy in lung cancer A549 cells. *BMC Cancer*, **20**, 634.
46. Qu,J., Liu,G.H., Huang,B. and Chen,C. (2007) Nitric oxide controls nuclear export of APE1/Ref-1 through S-nitrosation of Cysteines 93 and 310. *Nucleic Acids Res.*, **35**, 2522–2532.
47. Jedinak,A., Dudhgaonkar,S., Kelley,M.R. and Sliva,D. (2011) Apurinic/apyrimidinic endonuclease 1 regulates inflammatory response in macrophages. *Anticancer Res.*, **31**, 379–385.
48. Park,M.S., Lee,Y.R., Choi,S., Joo,H.K., Cho,E.J., Kim,C.S., Park,J.B., Jo,E.K. and Jeon,B.H. (2013) Identification of plasma APE1/ref-1 in lipopolysaccharide-induced endotoxemic rats: implication of serological biomarker for an endotoxemia. *Biochem. Biophys. Res. Commun.*, **435**, 621–626.
49. Li,M., Xiong,J., Yang,L., Huang,J., Zhang,Y., Liu,M., Wang,L., Ji,J., Zhao,Y., Zhu,W.G., *et al.* (2022) Acetylation of p62 regulates base excision repair through interaction with APE1. *Cell Rep.*, **40**, 111116.
50. Cao,X., Sun,Y., Lu,P. and Zhao,M. (2020) Fluorescence imaging of intracellular nucleases—a review. *Anal. Chim. Acta*, **1137**, 225–237.

**Received:** June 17, 2023. **Editorial Decision:** February 27, 2024. **Accepted:** March 7, 2024
© The Author(s) 2024. Published by Oxford University Press on behalf of Nucleic Acids Research.
This is an Open Access article distributed under the terms of the Creative Commons Attribution-NonCommercial License (http://creativecommons.org/licenses/by-nc/4.0/), which permits non-commercial re-use, distribution, and reproduction in any medium, provided the original work is properly cited. For commercial re-use, please contact journals.permissions@oup.com